

Obtaining stiffness exponents from bond-diluted lattice spin glasses

S. Boettcher and S. E. Cooke*

Physics Department, Emory University, Atlanta, Georgia 30322, USA

(Received 18 January 2005; revised manuscript received 23 March 2005; published 9 June 2005)

Recently, a method has been proposed to obtain accurate predictions for low-temperature properties of lattice spin glasses that is practical even above the upper critical dimension, $d_c=6$. This method is based on the observation that bond-dilution enables the numerical treatment of larger lattices, and that the subsequent combination of such data at various bond densities into a finite-size scaling ansatz produces more robust scaling behavior. In the present study we test the potential of such a procedure, in particular, to obtain the stiffness exponent for the hierarchical Migdal-Kadanoff lattice. Critical exponents for this model are known with great accuracy and any simulations can be executed to very large lattice sizes at almost any bond density, effecting an insightful comparison that highlights the advantages—as well as the weaknesses—of this method. These insights are applied to the Edwards-Anderson model in $d=3$ with Gaussian bonds.

DOI: 10.1103/PhysRevB.71.214409

PACS number(s): 75.10.Nr, 05.50.+q, 02.60.Pn

I. INTRODUCTION

The exploration of low-temperature properties of disordered systems remains an important and challenging problem.¹ Systems in this class possess a low-temperature glassy state with a glass transition at some temperature $T_g > 0$. They are characterized by a complex (free-)energy landscape in configuration space^{2–4} with a hierarchy of valleys and barriers whose multi-modal structure impedes the progression of any dynamics towards equilibration, causing tantalizing phenomena, such as trapping and jamming on intermediate time scales, and aging on long time scales. An understanding of such systems is of paramount importance as these phenomena are observed for a large class of materials as well as for biological systems.⁵

The paradigmatic model for the study of such phenomena is the Ising spin glass, either on a finite-dimensional lattice [Edwards-Anderson (EA) model⁶] or some other random network structure. Disorder effects arise typically via quenched random bonds, random local fields, or merely the randomness of the network itself, each can lead to conflicting constraints which leave variables frustrated. It is believed that a proper understanding of static and dynamic features of EA may aid a description of the unifying principles expressed in the wider class of realistic problems.⁷

Unfortunately, after 30 years of research there is still no consensus on whether the subtle mean-field picture for Ising spin glasses derived long ago^{8–10} has any relevance for real-world materials at low temperatures.¹¹ Progress towards such an understanding is slow due to the peculiar structure of the problem at hand. The intricate multimodal low-energy landscape puts the computational effort needed to determine thermodynamic observables usually into the class of NP-hard combinatorial optimization problems¹² known from computer science, for which worst case computational costs increase faster than any power of the system size. (Interestingly, it is in this area of computer science itself where the mean-field theory at $T=0$ has had a most significant impact so far.¹³)

Most insights into finite-dimensional systems has thus been gained through alternative computational approaches to elucidate low-temperature properties. Aside from methods

designed to expedite some thermodynamically correct algorithm, such as parallel tempering¹⁴ or the waiting time method,¹⁵ one focus area has been the use of optimization heuristics directed toward fully enumerating ground-state configurations by any means.^{5,16–20} These ground states should provide the basis for the thermodynamic behavior of the system at and near $T=0$. But due to the NP hardness, even heuristic methods become unreliable when system sizes exceed about $\approx 10^3$ variables, often too small to draw safe conclusions or to sufficiently discriminate between theoretical ideas.^{21,22}

This fact is illustrated by the determination of the stiffness exponent, often labeled y or θ ,^{7,23} a fundamental quantity assessing low-temperature energy fluctuations: a positive value of y , as found in EA for $d \geq 3$, denotes the increase in the energetic cost (i.e., “stiffness”) accompanying a growing number of variables perturbed from their position in the ground state. The rise in energetic penalty paid for stronger disturbances signals the presence of an ordered state. In turn, for systems with $y \leq 0$ such order is destabilized by arbitrarily small fluctuations.

In this paper, we will extract the stiffness exponent from the response induced through defect interfaces.²³ These can be created by fixing the spins along the two faces of an open boundary in one lattice direction. The ground state configuration with energy E_0 of an instance is first determined for a random fixing of those boundary spins, then the energy E'_0 is obtained for the same instance and the same fixing, but with all spins reversed on one of the faces. Hence, the interface energy $\Delta E = E'_0 - E_0$ created by the perturbation on the boundary is sampled, and its distribution $P(\Delta E)$ determined. If a system is glassy, the typical energy scale involved, here represented by the width of the distribution, $\sigma(\Delta E) = \sqrt{\langle \Delta E^2 \rangle - \langle \Delta E \rangle^2}$, should grow with the size of the perturbation, say, the linear extend of the boundary, L , as²³

$$\sigma(\Delta E) \sim L^y. \quad (1)$$

Accurate determination of this exponent in $d=3$ has long been elusive, with values given between $y \approx 0.19$ ^{17,23} to

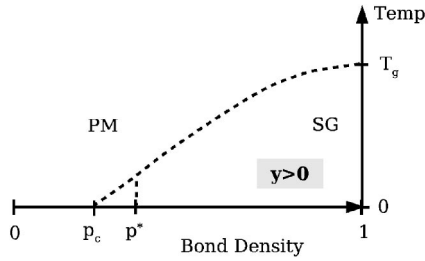


FIG. 1. Phase diagram for bond-diluted spin glasses at low temperatures. Lattice spin glasses of dimension $d \geq 3$ possess a spin glass phase (SG) below the glass transition temperature $T_g > 0$. This phase should persist even for diluted lattices, as long as the percolating cluster of connected spins is compact, i.e., for bond densities p sufficiently above p_c (Refs. 27, 28, and 33). Below p_c , the collection of small clusters can only respond paramagnetically (PM) on long length scales for any $T \geq 0$. Depending on the details of the bond distribution, the $T=0$ transition occurs at $p^* = p_c$ (continuous bonds) or at $p^* > p_c$ (discrete bonds), respectively determining the slope of the phase boundary $T_g(p)$ at p^* .

≈ 0.27 .²⁴ While it was save to say that $y > 0$, its value could be at best given as $y_3 = 0.2(1)$. In terms of sorting out theoretical models, this is too inaccurate to draw solid conclusions.²²

This limited accuracy originates with trying to fit data over too small a range of system sizes L . Scaling in this range is further beset by slowly decaying corrections in L which make it hard to decide even where scaling sets in.^{25,26} The remedy proposed then is to possibly extend scaling by considering *bond-diluted* lattices.^{27–29} As has been argued already in Ref. 33, as soon as the percolation window for bond densities $p > p_c$ has been exceeded at some lattice size, the long-range properties of the giant component—and hence, of the spin glass defined on it—are essentially compact, representing the $T=0$ fixed point of the fully connected lattice. This implies that there the exponent y is independent of the bond density p . These features of bond-diluted glasses are summarized in the phase diagram in Fig. 1. The independence of y from p appears to hold also for Gaussian bonds in $d=2$,³⁰ where $y < 0$ (no spin glass phase) and universality with respect to bond disorder is violated.^{26,31,32}

While we focus on the defect energy at $T=0$ here, bond dilution may also be an effective means to study other observables.³⁴ For determining $T=0$ properties, this approach makes the treatment of larger lattices sizes practical in as much as exact algorithms can be devised that allow the elimination of a large number of variables, whose state becomes entrained to other variables in a predictable way in the ground state.³⁵ In this way, systems with more than 10^6 variables have been “reduced” to remainder graphs consisting of no more than a few hundred variables that are amenable to standard optimization methods.²⁷ Clearly, though, due to those almost trivial variables, the information content about the asymptotic behavior captured by such graphs may be limited, and a price has to be paid through extended transient behavior. As we hope to demonstrate here, in the end much is gained in this method, although at the extremely large lattice sizes that can be reached with the Migdal-Kadanoff approximation used here, diminished returns are obtained because of

a lack of knowledge on how scaling corrections vary with bond density.

As we will recount in Sec. III, Refs. 33 and 36 suggest to generalize Eq. (1) to

$$\sigma(\Delta E)_{L,p} \sim \xi(p)^{y_p} \left(\frac{L}{\xi(p)} \right)^y f \left(\frac{L}{\xi(p)} \right), \quad (2)$$

for $L \gg 1$ and $\xi(p) \sim (p-p^*)^{-\nu^*} \gg 1$. The scaling function f was chosen to be constant for $L \gg \xi(p)$. The limit $p \rightarrow p^*$ towards the $T=0$ transition between the spin glass and paramagnetic regime (see Fig. 1) is interesting in its own right, and will be investigated further in Ref. 37. Yet, to elucidate properties of the glassy regime, the “window of opportunity” for our method appears to be at intermediate bond densities: p has to be sufficiently smaller than unity for our reduction algorithm to be efficient, but also sufficiently *above* p^* to attain system sizes $L \gg \xi(p)$. Analyzing our numerical data here suggests that in this window the condition $\xi(p) \sim (p-p^*)^{-\nu^*} \gg 1$ assumed in Eq. (2) does not hold, making $\xi(p)$ a more general function of p with unknown corrections to its singular part.

Operationally, we thus propose a naive ansatz for a collapse of the numerical data valid for the asymptotic regime $L \gg \xi(p) \sim 1$ only,

$$\sigma(\Delta E) = f(\infty)x^y \quad [x = L(p-p^*)^{\nu^*}]. \quad (3)$$

Since the numerically accessible data appears to violate $\xi(p) \gg 1$, the parameters p^* and ν^* here merely facilitate the data collapse by fitting a more general function $\xi(p)$, and can not be expected to yield accurate predictions for the critical values in Eq. (2). The successful implementation of this ansatz for the Migdal-Kadanoff hierarchical lattice here lends credibility to the findings for y_d of the EA in Refs. 27 and 28.

Finally, it is remarkable that this approach works substantially better for a discrete $\pm J$ bond distribution than for Gaussian bonds, for which scaling corrections due to a small $\xi(p)$, and even due to finite- L transients, are far more significant. Just as for the $\pm J$ data, the similarity between our Migdal-Kadanoff and our EA data with Gaussian bonds presented here is striking. While this issue eventually deserves more thorough investigation, we can speculate on the origin of these strong transients. One may remember that in $d=1$, $\sigma(\Delta E) \sim L^{-1}$ for continuously distributed bonds with finite $P(0)$, while $\sigma(\Delta E) \sim L^0$ for $\pm J$ bonds. The interface may settle on the extremely weakest within a more widely distributed set of continuous bonds, while for $\pm J$ it *must* break a bond of order unity. Similarly, on short ranges in higher dimensional lattices, particularly dilute ones, with a Gaussian distribution peaked at $J=0$, the violation of heavy bonds can be deferred *initially* which an extended defect eventually demands on larger scales L . This naive argument is supported by the fact that at equal p and L , defect energies $\sigma(\Delta E)$ are typically somewhat smaller for Gaussian than for $\pm J$ bonds, as will be seen in Fig. 3.

In the next section we introduce the Migdal-Kadanoff hierarchical lattice, followed in Sec. III by a discussion of the scaling arguments leading to Eq. (2) and to our ansatz in Eq.

(3) used to obtain the stiffness exponent on bond-diluted lattices. Section IV contains our discussion of the Migdal-Kadanoff data, followed by the application of the gained insights to the diluted EA with Gaussian bonds in Sec. V. Finally, Sec. VI contains our conclusions.

II. MIGDAL-KADANOFF HIERARCHICAL LATTICE

To test the scaling ansatz in Eq. (3) for the stiffness exponent, we consider here the bond-diluted hierarchical lattice (see Fig. 2), obtained in the Migdal-Kadanoff bond-moving scheme³⁸ for low-dimensional spin glasses. These lattices have a simple recursive yet geometric structure and are well studied.^{25,33,39,40} Most importantly, their ground states can be obtained in polynomial time at any bond density, and we can discuss our results independent of any systematic bias introduced by a subsequent optimization process that may be required for more complicated models like EA.³⁵ A most interesting property of these lattices is the curious fact that the scaling of its defect energy distribution, giving rise to the stiffness exponent, behaves in all respects very similar to that measured for actual three-dimensional lattices.^{7,23,40}

To generate a hierarchical lattice, starting from generation $I=0$ with a single link, at each subsequent generation I all links from $I-1$ are replaced with a new subgraph, as described in Fig. 2. The structure of the subgraph arises from the Migdal-Kadanoff bond-moving scheme in d dimensions, and has $2^d=8$ links for $d=3$ here. Thus a hierarchical lattice of generation I has $(2^d)^I$ links (if undiluted), thus corresponding to a d -dimensional lattice of “length” $L=2^I$ and $n=2+2^{d-1}(L^d-1)/(2^d-1)=O(L^d)$ vertices. While the average connectivity is $\sim 4-2^{2-d}$, the two root vertices from generation $I=0$ themselves obtain in generation I a connectivity of $\sim 2^{(d-1)(I-1)}$. In turn, $\sim 2^{dI-1}$ vertices, 7 in 8 for $d=3$, are only two-connected.

The diluted hierarchical lattice percolates when there is a path between the two root-vertices, representing the boundaries of the system. This notion leads to a simple recursion relation for the percolation threshold by counting the weights of all diluted subgraphs from Fig. 2 that percolate, i.e., connect right and left vertex. In $d=3$ one gets

$$p_{I+1} = 4p_I^2 - 6p_I^4 + 4p_I^6 - p_I^8, \quad (4)$$

which has a nontrivial stationary point at $p_c=0.2818376366$. There can not be long-range correlated behavior, such as spin glass ordering, for any $p \leq p_c$. It has been pointed out by Ref. 33 that a spin glass on a hierarchical lattice with $\pm J$ bonds exhibits a critical transition between a paramagnetic and a spin glass phase for bond densities at $p^*=0.31032$. While below p_c disconnected clusters clearly prevail and prevent long-range correlations, even for $p_c < p < p^*$ such correlations remain suppressed due to the cooperative behavior in the bond structure pervasive in the lattice, leading to cancellations that additionally disconnects subgraphs at some higher level of the hierarchy. In contrast, for a continuous bond distribution, such as the Gaussian bonds discussed below, any such cancellations would be unlikely, leading in this case to $p^*=p_c$.

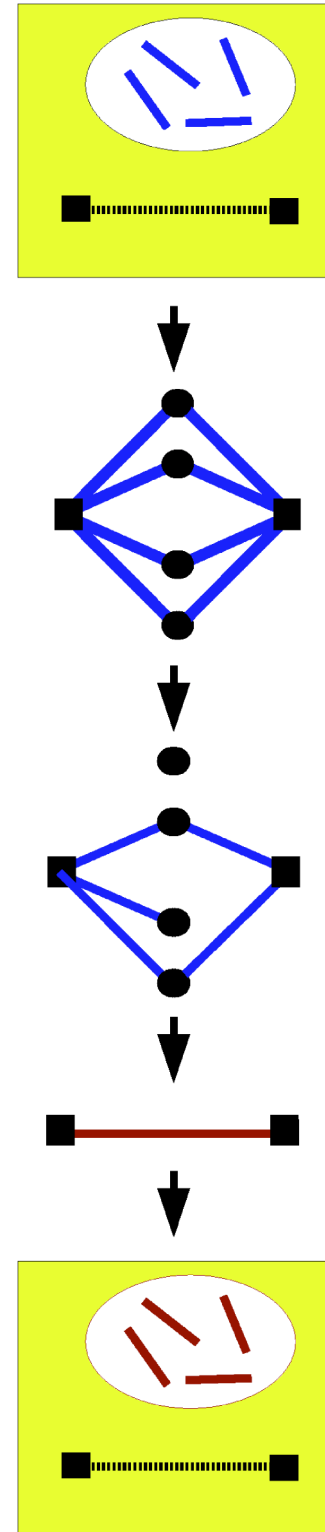


FIG. 2. Diagram for the recursive algorithm to calculate spin glasses on hierarchical lattices. Drawing bonds J_{I-1} randomly from a sufficiently large pool $P_{I-1}(J)$ at generation $I-1$ (top), a lattice of generation I is formed, then bond-diluted to density p , and finally “reduced” (Ref. 35) to an effective bond J_I between the root spins (squares), which is added to the pool $P_I(J)$ (bottom).

III. DEFECT-ENERGY SCALING FOR $p \rightarrow p^*$

Following the discussion in Refs. 33 and 36, for bond-diluted lattices at $p \rightarrow p^*$ we have to generalize the scaling relation in Eq. (1) for the defect energy to

$$\sigma(\Delta E)_{L,p} \sim \mathcal{Y}(p)L^\nu f\left(\frac{L}{\xi(p)}\right), \quad (5)$$

where $\mathcal{Y} \sim (p-p^*)'$ is an effective surface tension and $\xi(p) \sim (p-p^*)^{-\nu^*}$ is the correlation length for the crossover into glassy behavior. Note that Eq. (5) requires both, L and ξ , to be large compared with the unit lattice spacing to avoid further scaling corrections. The scaling function $f(x)$ is defined to be constant for large argument, $L \gg \xi \gg 1$.

For $\xi \gg L \gg 1$, Eq. (5) requires that $f(x) \sim x^\mu$ for $x \rightarrow 0$ to satisfy either the vanishing of σ with L in case of $p^* = p_c$ (Gaussian bonds), or its scale invariance at a $p^* > p_c$ ($\pm J$ bonds). Clearly, due to the tenuous fractal nature of the percolating cluster at $p^* = p_c$, no long-range order can be sustained, defects possess a vanishing interface, and one may expect that

$$\sigma(\Delta E)_{L,p^*} \sim L^{y_p}, \quad (6)$$

where $y_p \leq 0$.³⁶ To cancel the p -dependence at $p = p^*$, Eq. (5) requires $y + \mu = y_p$ and $t + \mu\nu = 0$, i.e., $t = \nu y + \phi$, setting $\phi = -\nu y_p$.³⁶ As a result, we obtain Eq. (2). In contrast, for $p^* > p_c$, the percolating cluster appears compact on scales $L \gg (p^* - p_c)^{-\nu}$, and σ can not vanish for further increasing L . Yet, neither can σ increase at p^* , by definition. Hence, σ remains scale invariant, and correspondingly ϕ and y_p vanish in Eqs. (2) and (6) for $\pm J$ bonds.

In the case of continuous bond distributions $P(J)$ with finite $P(0)$, where $p^* = p_c$, spin glass ordering can only be noticed on scales at least as large as the correlation length $\xi \sim (p - p_c)^{-\nu}$ associated with percolation, suggesting $\nu^* = \nu$. In case of $\pm J$ bonds, the cooperative cancellations between discrete bonds mentioned above further weaken order, leading to $\nu^* > \nu$ for the $T=0$ glass transition at p^* . Accordingly, Ref. 33 finds $\nu = 1.2274$ and $\nu^* = 1.5373$ for the hierarchical lattice in $d=3$.

Finally, at the crossover $\xi \sim L$, where the range L of the energy excitations $\sigma(\Delta E)$ reaches the percolation length and spin glass order ensues, Eq. (5) yields

$$\sigma(\Delta E)_{\xi(p),p} \sim (p - p^*)' \xi^y f(1) \sim (p - p^*)^\phi. \quad (7)$$

One can associate a characteristic temperature with this crossover by $\beta\sigma(\Delta E)_{\xi(p),p} \sim 1$; for temperatures above this $T = 1/\beta$, thermal fluctuations destroy spin glass order. This suggests a relation between bond density and the glass transition temperature:

$$T_g(p) \sim (p - p^*)^\phi. \quad (8)$$

Equation (8) defines ϕ as the ‘‘thermal-percolative crossover exponent,’’³⁶ which specifies the details of the phase boundary near p_c (or p^*) in Fig. 1. For the continuous distribution, where $p^* = p_c$, ϕ would be in general nontrivial, while for $\pm J$ at $p^* > p_c$ it appears that $\phi = 0$, indicating a jump in the phase boundary $T_g(p)$ at p^* .

The exponent ϕ could be of importance, since it may be experimentally accessible^{41,42} while the relation $\phi = -y_p\nu$ provides a simple computational determination in terms of Eq. (6) and the well-known percolation exponents ν . This connection will be considered in a forthcoming publication.³⁷

In the following, we will explore some of these relations numerically for the hierarchical lattice, for which large sizes L can be obtained. But the central purpose of this paper is to probe Eq. (3), which has been used in Refs. 27 and 28 to provide accurate predictions for the stiffness exponents y_d , fundamental for describing low-temperature excitations in spin glasses.

IV. NUMERICAL RESULTS FOR HIERARCHICAL LATTICES

Our numerical studies on the hierarchical lattice have been conducted with the algorithm described in Ref. 35. It is based on the evolution of bond pools (see Fig. 2) of size A_I from generation I to generation $I+1$, similar to the procedure already used in Refs. 23 and 43. In our algorithm, though, an existing bond at generation I is replaced with a new bond (to keep A_I constant) for every k new bonds that are added at generation $I-1$. This procedure is legitimate in principle, as even neighboring subelements in the graph act independently and only effect each other in a collective sense just as represented by the bonds replacing them in the next generation. The danger is that the diversity in the pool of those bonds is insufficient, leading to creeping spurious correlations and difficult-to-perceive drifts away from the true values of observables. Since the size of the pool of bonds has only a minor effect on the computational effort for $k=1$, we can rerun the same calculation repeatedly to a high number of generations using ever-larger pool sizes A_I until the data becomes insensitive to A_I . We have used this procedure to generate most of the data in Fig. 3.

Further problems arise when we use this algorithm near the critical point p^* . There, the bond distribution is torn between the trivial fix point of vanishing width in the paramagnetic phase and the true glassy state with subtle, long-range correlations between bonds of the previous and following generations, and small fluctuations can severely bias the evolution. At that point, we have to resort to slower regeneration rates with $k > 1$, or even the exact algorithm for which $k = 2^d$.

Our numerical studies, as shown in Fig. 3, confirm the picture described in Sec. III. To induce an interface in the MK as described in the Introduction we consider only the leftmost and the rightmost spin in each graph as entire boundary. This is meaningful, since each of these spins connects to $O(L)$ other spins, see Sec. II. Then, the defect energy of a lattice at generation $I-1$ (size $L = 2^{I-1}$) is simply (twice) the value of the bond of generation I replacing that graph (see Fig. 2). In this sense, the defect energy $\sigma(\Delta E)$ can be interpreted as an effective coupling between both sides of the defect interface,³⁶ if that coupling strengthens with distance L , the system is in an ordered state, and vice versa.

Note that in Fig. 3 for $p < p^*$ the data evolves towards the $p=0$ fixed point with $\sigma(\Delta E) = 0$, while for $p > p^*$ it invariably

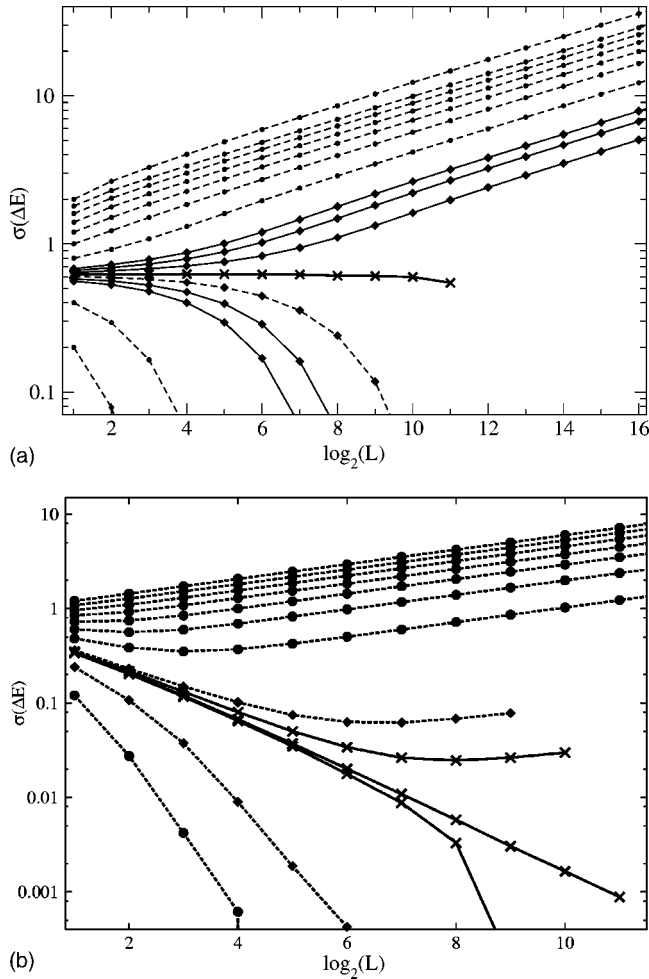


FIG. 3. Plot of the width $\sigma(\Delta E)$ of the defect energy distribution as a function of systems size L for various bond fractions p using discrete bonds (top) and Gaussian bonds (bottom) in the $3d$ Migdal-Kadanoff lattice. In each plot, dashed lines from bottom to top refer to $p=0.1, 0.2, \dots, 1$. Solid lines refer to data with $p=0.28, 0.29, \dots, 0.34$ on top, and $p=0.28, 0.2818$, and 0.29 on the bottom. In both plots, the data points with circles were obtained using the $k=1$ implementation from Ref. 35, those with diamonds using $k=2$, and those with crosses near the respective p^* required the exact algorithm. Note that at $p^* \approx 0.3103 > p_c$ on top, the slope is near vanishing, while for $p^* = p_c = 0.2818$ on the bottom, the slope indicates a well-pronounced power-law decay.

evolves to the $p=1$ fixed point with scaling behavior $\sigma(\Delta E) \sim L^\nu$. Figure 3 clearly suggests that $p^* = p_c = 0.2818$ for the continuous Gaussian bond distribution, while the discrete $\pm J$ bond distribution favors $p^* = 0.3103 > p_c$. At p^* , σ varies distinctively different with L than even for bond densities p quite near to p^* . In particular, the behavior of σ at the respective p^* appears to confirm the predictions for the scaling in Eq. (6) with $y_p=0$ (i.e., $\phi=0$) for discrete bonds, and a nontrivial exponent we measure to be about $y_p = -0.9(1)$ for Gaussian bonds.

In the following, we want to test the predictive power of the finite-size scaling ansatz in Eq. (3) as argued on the basis of Eq. (2). This ansatz has been applied to the numerical measurements of the glassy state ($p > p^*$) on large, bond-

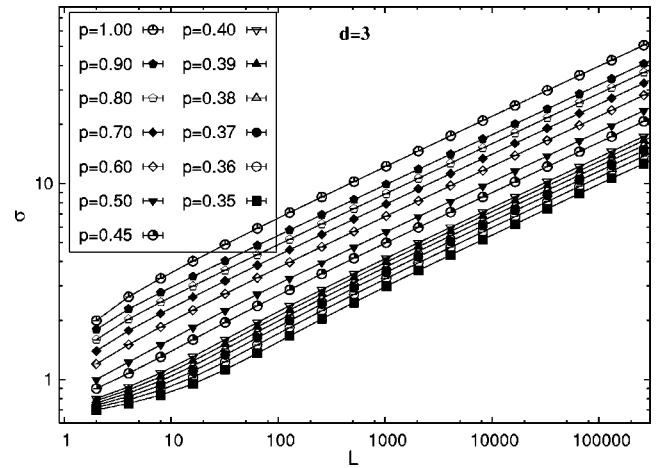


FIG. 4. Plot of the raw data for $\sigma(\Delta E)$ as a function of systems size L for bond fractions $p^* < p \leq 1$ using discrete $\pm J$ bonds. Some of this data is already shown in Fig. 3. Of note is that there appears to be no variation with p in the asymptotic scaling, that scaling corrections at small L are least noticeable for intermediate p , and that there is an anomalous gap between data for $p=0.9$ and $p=1$.

diluted lattices as recently proposed in Refs. 27 and 28. In this scheme, the properties of the zero-temperature fixed point are determined for a number of intermediate bond-densities p —sufficiently above p^* to be glassy and sufficiently small to achieve large system sizes L . In particular, Refs. 27 and 28 focused on the defect energy for finite dimensional lattices. This procedure should be applicable also to other observables.

First, we consider $\pm J$ bond distributions, which had been used exclusively in Refs. 27 and 28. In Fig. 4 we plot without any scaling all data we have obtained with the method above for $p=0.35, \dots, 1$. It is worth mentioning two features of that data: (1) scaling corrections for smaller L appear to change sign at around $p \approx 0.45$, suggesting that those corrections are weakest at intermediate values of p instead of at $p=1$, against expectation. (2) The data for $p \rightarrow 1$ initially narrows (on this logarithmic scale) for equal increments ($\Delta p=0.1$), but then exhibits an increased gap in the jump from $p=0.9$ to $p=1$. Both of these features have also been observed for the EA data in $d=3$.^{27,28} The first feature seems insignificant here for data extending out to $L > 10^5$, but the suppression of scaling corrections becomes extremely helpful when the maximal attainable L is small, as for the EA model. This fact has also been exploited in Ref. 34. The second feature could be explained with the requirement for the scaling ansatz of $\xi \sim (p-p^*)^{-\nu} \gg 1$, which may not be satisfied for any p too far from p^* . In Ref. 35, similar rapid variations in an observable (the overlap) for $p \rightarrow 1$ have been observed, although a connection to the variations in the amplitude of σ here is not clear.

For this discrete bond distribution, the scaling ansatz in Eq. (2) simplifies, since we can assume $y_p=0$; see top of Fig. 3. Hence, we fit the data obtained for various bond densities $p > p^*$ in Fig. 4 directly to the form proposed in Eq. (3), where the scaling variable x is adjusted to provide the best data collapse. The unknown scaling function $f(x)$ has been

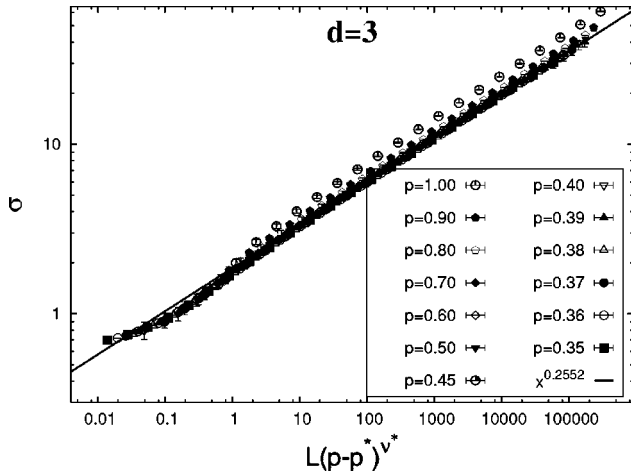


FIG. 5. Collapse of the data from Fig. 4 according to the scaling ansatz in Eq. (3), but using the exactly known values for p^* , ν^* , and $y=0.2552$. Here, only $f(\infty)$, an overall amplitude, remains as a free fitting parameter.

replaced by a fitting constant, $f(\infty)$, to capture its leading asymptotic behavior for large L .

The advantage of the hierarchical lattice is that we already know the expected values for the parameters involved in such a fit, i.e., $p^*=0.31032$, $\nu^*=1.5373$,³³ and $y \approx 0.2552$.^{35,43} Thus, first we can attempt to utilize this knowledge to collapse the data in Fig. 4 by fixing p^* , ν^* , and y , only leaving $f(\infty)$ to be fitted. As can be seen in Fig. 5, the data collapses exceedingly well even for small x , as long as p is not too large. Scaling ensues quickly for $x > 1$, which would allow for an excellent fit, *if* one were to exclude data for $p > 0.7$. Remarkable is the quality of the collapse for data reaching below $x < 1$. It reveals a concave shape for $f(x)$, which explains the finite-size corrections in Fig. 4: Data with lower p first rises slowly, then more rapidly for increasing L , before scaling settles in. In turn, data with higher p immediately rises rapidly before settling into a slower asymptotic growth. Data with p near unity rises even more rapidly to overshoot the collapse in the scaling regime.

Clearly, these observations about the intricacies of $f(x)$ are far too subtle to be of any use in the more typical situations where we have no prior knowledge of the parameters. Worse yet, even with that knowledge, corrections due to the finite size of $\xi=(p-p^*)^{-\nu^*}$ in particular appear to prevent a collapse of the data in much of the asymptotic scaling regime. Yet, it seems obvious that the data for *all* $p > p^*$ and large enough L exhibits scaling according to Eq. (1), providing information we desire to exploit. The precise value of the parameters p^* and ν^* are important for the behavior of $f(x)$ near $x \sim 1$, but have little effect on the scaling behavior for $x \gg 1$. Thus, instead of correcting the fit to extract accurate values for all parameters, we cut data that does not appear to scale well. Then, we can collapse the data in the scaling regime according to Eq. (3), merely using p^* , ν^* , and $f(\infty)$ as free parameters to facilitate an accurate determination of y only.

Figure 6 displays the same data as before, but only data judged by inspection to be sufficiently scaling ($L > 1024$ at

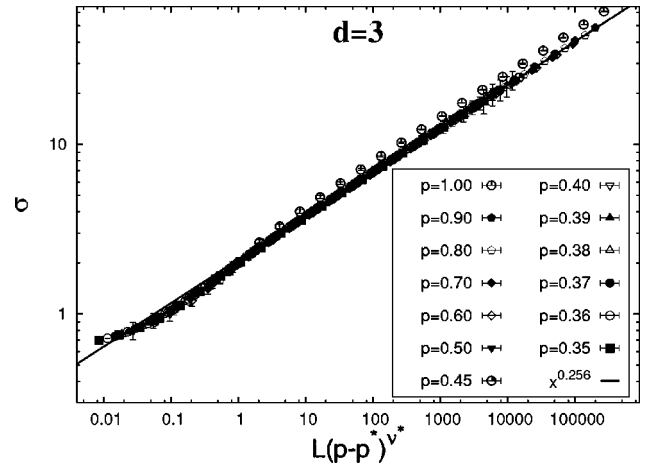


FIG. 6. Collapse of the data from Fig. 4 according to the scaling ansatz in Eq. (3). Here, the values for $f(x)$, p^* , ν^* , and y are all determined from the fit of data in the scaling regime only, although all data is displayed.

$p=0.35$ down to $L > 8$ for $p=0.9$, see Fig. 4) has been used for the fit. *All* data for $p=1$ has been explicitly excluded due to the anomalous jump in the amplitude of σ noted in Fig. 4. These choices are reflected in the collapse: All but $p=1$ data combines exceedingly well for $x \gg 1$, predicting $y=0.256(1)$, only 1/2% above the exact value. For data scaling over almost 5 decades, one may have expected more accuracy for y , but slowly decaying scaling corrections,³⁵ and the smallness of y itself, limit the relative accuracy. The value for y remains quite robust under changes in the data points included in or excluded from the fit. On the other hand, the fit selects $p^* \approx 0.29$, $\nu^* \approx 1.94$, and $f(\infty) \approx 2.1$. Note that the fitted value for ν^* is larger than the actual value. It is this increase in ν^* that facilitates the collapse of the data in the asymptotic regime, $x \gg 1$. Consequently, the collapse of the data excluded from the fit at $x \leq 1$ is somewhat poor (but still not too bad here). This is exactly the approach adopted in Refs. 27 and 28 to extract the best possible estimate for y . Hence, as noted there, the values for any parameter aside from y fitted in this way must be treated with caution.

We can proceed in a similar manner for the bond-diluted hierarchical lattice with a continuous Gaussian bond distribution. First, we plot the raw data obtained with the algorithm described above in Fig. 7. In this case, finite-size corrections are more pronounced but appear to diminish more gradually towards $p=1$. The scaling arguments from Sec. III would suggest to fit the data to a form derived from Eq. (2),

$$\frac{\sigma(\Delta E)_{L,p}}{(p-p^*)^\phi} \sim f(\infty)x^y. \quad (9)$$

Here, it appears that the scaling collapse involves yet another parameter, the thermal-percolative crossover exponent ϕ for the scaling variable $x=L/\xi(p)$ at $p \rightarrow p^*=p_c$. In contrast to p^* and ν^* , which can be determined analytically for the hierarchical lattice, ϕ is similarly nontrivial as y itself, and is even harder to estimate numerically. By definition, $\phi = -\nu_p$ and y_p has to be obtained exactly at $p=p^*$, see Eq. (6), where the

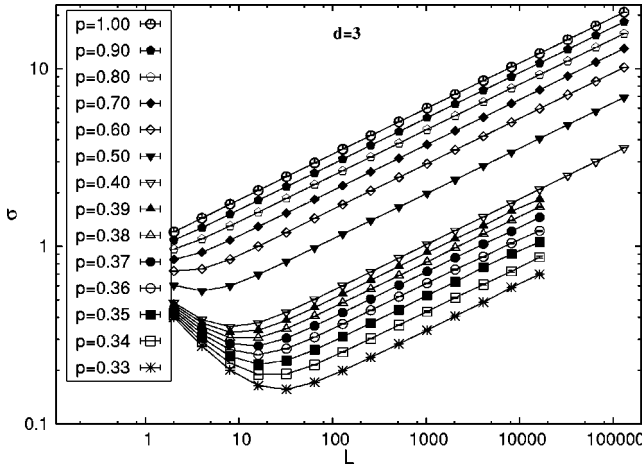


FIG. 7. Plot of the raw data for $\sigma(\Delta E)$ as a function of systems size L for bond fractions $p^* < p \leq 1$ using continuous Gaussian-distributed bonds. Some of this data is already shown in Fig. 3.

algorithm is the most delicate, limiting us to $L \leq 2^{11}$. As shown in Fig. 3 (bottom), from the data for σ at p^* we can extract $y_p = -0.9(1)$. With the percolation exponent, $\nu = 1.22$, we obtain $\phi = 1.1(1)$.

In Fig. 8, we collapse the data from Fig. 7 using Eq. (9) by fitting $f(\infty)$ and ϕ , but holding p^* and ν^* , and y fixed. Similar to Fig. 5, the collapse proceeds well for data that is near $x \sim 1$ and has p near p^* . Already for intermediate values of p , the data spreads widely, suggesting that $\xi(p)$ is too small there. We obtain a fitted value of $\phi \approx 0.9$, not too far from the determination via y_p above.

Again, the focus on properties associated with p^* gave us a good collapse near $x \sim 1$, but not about the desired asymptotic scaling regime for y at $x \gg 1$. Consequently, we again exclude all data in the fit that is by inspection of Fig. 7 not yet in that asymptotic regime and proceed with an unrestricted fit involving all parameters. The result of such a collapse is shown in Fig. 9. Now the data collapse is excel-

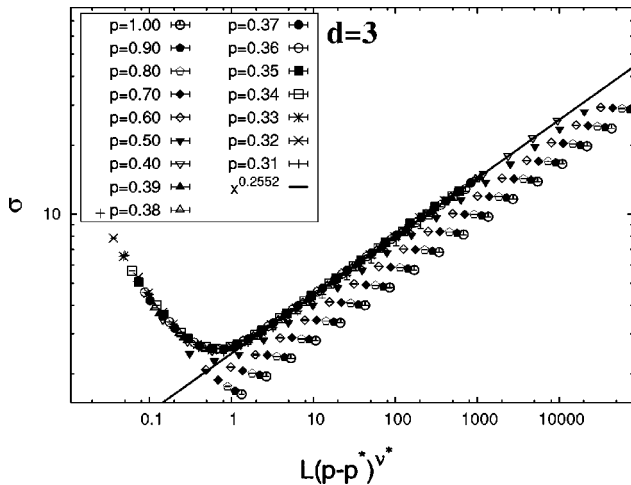


FIG. 8. Collapse of the data from Fig. 7 according to the scaling ansatz in Eq. (9), but using the exactly known values for p^* and ν^* (then y is not needed). Here, only $f(\infty)$ and ϕ remain as free fitting parameters.

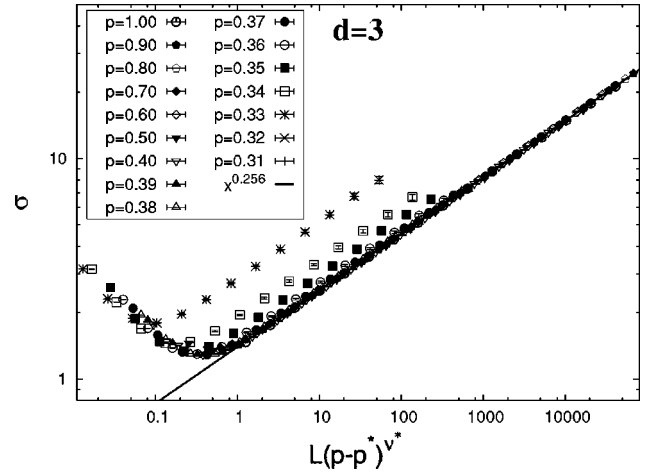


FIG. 9. Collapse of the data from Fig. 7 according to the scaling ansatz in Eq. (9). Here, the values for $f(x)$, p^* , ν^* , ϕ and y are all determined from the fit of data in the scaling regime only.

lent in the asymptotic regime for data of sufficiently large L and large enough p , including $p=1$, but poor near $p=p^*$ and for $x \leq 1$ for the excluded data. The fitted values here are $p^* \approx 0.32$, $\nu^* \approx 1.20$, $\phi \approx 0.51$, and $y \approx 0.256$, again within 1/2% error of the value directly determined at $p=1$. Surprisingly, even ν^* is well approximated now while only ϕ is substantially off. In fact, ignoring the correction in the scaling behavior due to the exponent ϕ (i.e., $\phi=0$), the data collapse proceeds even more favorably, giving $y=0.2557$ but $p^*=0.31$ and $\nu^* \approx 3$. Having one less free parameter makes the data collapse a bit more robust, with ν^* picking up the error due to a less adequate scaling ansatz. That a collapse of the data succeeds even when we ignore ϕ is a reflection of the fact that in the limit of large argument for f , only two of the three exponents y , ϕ , and ν^* are independent. Equation (9) reduces to $\sigma \sim f(\infty)L^y(p-p^*)^{\phi+y\nu^*}$, and setting $\phi=0$ leads us right back to Eq. (3).

V. EDWARDS-ANDERSON MODEL WITH GAUSSIAN BONDS

We have already pointed out the striking similarities between the data for defect energies on $d=3$ hierarchical lattices here and on cubic lattices in Refs. 27 and 28 for $\pm J$ bonds. We complement this comparison here with a study of the EA on cubic lattices with Gaussian bonds. Such a study allows us to probe some of the assertions leading to Eq. (3). It also tests the universality of y with respect to the details of the bond distribution. The well-known result for $d=1$ mentioned in the Introduction and recent studies for $d > 1$,^{26,31,32} have shown that there are significant differences in the results for the stiffness exponent with respect to bond distribution below the lower critical dimension, where $y < 0$, while Ref. 32 has argued that universality should hold when $y > 0$. Our findings here, and for the hierarchical lattice above, support this point.

Unlike for hierarchical lattices, the numerical effort required to achieve any reasonable system size L in the determination of defect energies on cubic lattices grows exponen-

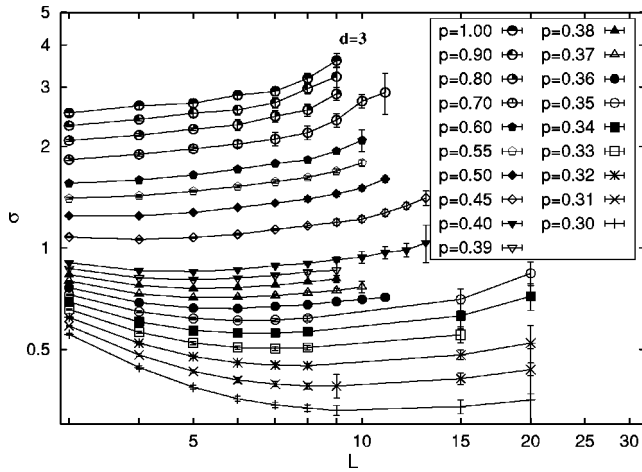


FIG. 10. Plot of the raw data for $\sigma(\Delta E)$ as a function of systems size L for bond fractions $p_c = p^* < p \leq 1$ using continuous Gaussian-distributed bonds on a cubic lattice. At nearly each p , long transients are followed by an intermediate scaling regime, cut short at larger L , when numerical inaccuracies result in a systematic drift.

tially with the number of variables; the problem is NP hard.¹² While the method of reducing low-connected variables is applicable just as well for the Gaussian distribution, our implementation of the extremal optimization heuristic does *not* perform well for these systems. Although it might be capable to yield reasonably accurate predictions for ground states themselves, we notice a significant drift in the data for the defect energy, formed out of the difference between two closely related ground states, starting with remainder graphs of size $n \geq 250$. As Fig. 10 shows, much of the obtained data, both for small and larger L , is not scaling and has to be discarded. We note that the long transients even before any asymptotic scaling is reached for small L is again reminiscent of the hierarchical lattice as in Fig. 7.

An attempt to collapse the data according to Eq. (9) as before requires the additional effort in determining y_p from Eq. (6). A determination of the defect energy at p_c has the advantage that the exact reduction method almost always succeeds completely, obviating the application of any optimization and large lattice sizes can be reached.³⁷ Our preliminary studies for systems up to $L=100$ have yielded an exponent of $y_p = -1.28(2)$. The consensus of results for the correlation exponent in $d=3$ for percolation seems to be $\nu = 0.86(2)$,⁴⁴ which results in a thermal-to-percolative crossover exponent, see Eq. (8), of $\phi = 1.10(4)$. Note that while $\nu < 1$ and $|y_p| > 1$ here, opposite to the hierarchical lattice in Sec. IV, the values of ϕ are indistinguishable within errors.

Similar to Fig. 8, one may try to collapse the data according to the scaling ansatz in Eq. (9) by fixing p^* , ν^* , and y to their best-known values and fitting for $f(\infty)$ and ϕ . Such a fit does not converge. We managed only to collapse the data for $p \rightarrow p^*$ by hand with the best-known value for $p^* = p_c \approx 0.248$,⁴⁵ but $\nu^* \approx 0.75$, and $\phi = 0.9$, somewhat below their best-known values. The result in Fig. 11, while far less convincing for this limited data set, parallels that in Fig. 8 to a large extent.

Finally, we set $\phi=0$, which reverts Eq. (9) into Eq. (3), and eliminate all data that is obviously not scaling. Pursuing

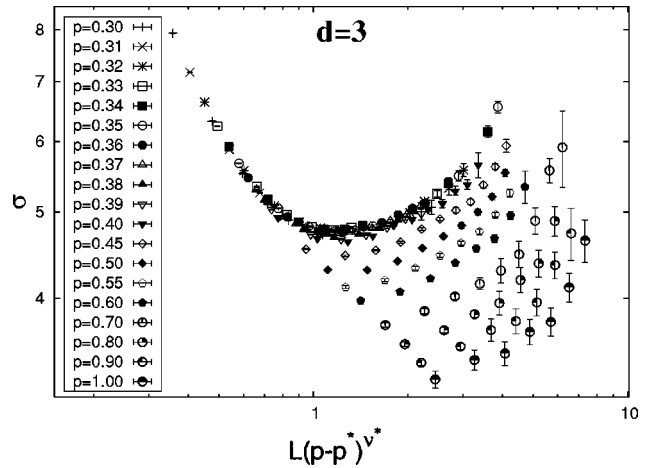


FIG. 11. Collapse of the data from Fig. 10 according to the scaling ansatz in Eq. (9). The values for the parameters had to be fixed by hand at $p^* = p_c \approx 0.248$, $\nu^* \approx 0.75$, and $\phi = 0.9$.

a fit of the remaining data according to Eq. (3) in the asymptotic regime, $x \gg 1$, without fixing any parameters, Fig. 12 is obtained. The result is noisy and apparently unsatisfactory: The value of $\nu \approx 3.1$ is as large as for Fig. 9, which separates this data in the scaling regime for each p into almost disconnected groups. Yet, the fit obtains a value of $y \approx 0.23$, in reasonable agreement with the best-known value of $y = 0.24(1)$.^{27,28}

Clearly, as for the hierarchical lattice at the end of Sec. IV, the focus on data with $x \gg 1$, i.e., p sufficiently larger than p^* such that $L \gg \xi(p)$, makes the details of the transition at $p \rightarrow p^*$ (such as the value of ϕ) irrelevant for the determination of y . This suggests Eq. (3) as the appropriate scaling ansatz to extract y , as proposed in Refs. 27 and 28, even for Gaussian bonds.

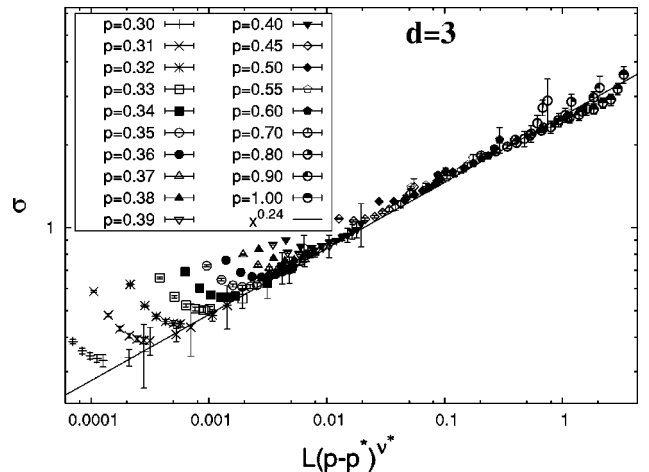


FIG. 12. Collapse of the data from Fig. 7 according to the scaling ansatz in Eq. (3), i.e., $\phi=0$. Here, the values for $f(\infty)$, p^* , ν^* , y are all determined from the fit of data in the scaling regime only, although all data from Fig. 7 are shown. Despite the obvious shortcomings of the data, the fitted value of $y \approx 0.23$ compares reasonably well with the best-known value of $y = 0.24(1)$ (Refs. 27 and 28), drawn here for reference (line).

VI. CONCLUSIONS

We have explored a recently proposed method of collapsing data obtained on bond-diluted lattices to estimate low-temperature scaling properties for the Edwards-Anderson model. Using bond-diluted hierarchical lattices from the Migdal-Kadanoff bond-moving scheme in $d=3$, for which many properties at $T=0$ are known exactly or with high accuracy, the validity of the method is probed. The data obtained for the defect energy of the hierarchical lattice proves to exhibit the same qualitative features as the—much more limited—data for the EA, respectively for discrete and continuous bond disorder.

The scaling ansatz used to collapse the data, most generally Eq. (2), was proposed in the neighborhood of a $T=0$ phase transition at bond density p^* between paramagnetic and spin glass behavior, which is closely associated with the bond percolation transition at p_c .^{33,36} Equation (2) requires both, the divergence of the system size L and of the correlation length $\xi=(p-p^*)^{-\nu^*}$. In contrast, the desired scaling behavior is associated with a $T=0$ fixed-point characteristic of the entire spin glass regime for $L \gg 1$, independent of $\xi(p)$ as long as $L \gg \xi(p)$. In particular, valuable data obtained for large L but intermediate values of p , for which $\xi(p)$ remains small, would have to be discarded in an ansatz based on $p \rightarrow p^*$. Thus, a naive ansatz, Eq. (3), based on the limit $L \gg \xi(p)$ (i.e., $x \rightarrow \infty$) in Eq. (2), exploits the obtained numerical data optimally (after data with $x \leq 1$ is cut). This ansatz is “naive” in the sense that $x=L(p-p^*)^{\nu^*}$ is not a true scaling variable, and the obtained values of the fitted parameters do not correspond to those defined by Eq. (2). Those parameters provide useful degrees of freedom in the fit to remedy unknown corrections in $\xi(p)$, as our discussion here shows. In fact, Eq. (3) has been used successfully in Refs. 27, 28, and

30, where very robust scaling behavior was extracted for the desired defect scaling exponent γ , but unrecognizable values have been found for p^* and ν^* . Unknown corrections in particular prevented a data collapse for data at $p=1$ there, a fact closely mirrored by the hierarchical lattice with a discrete bond distribution here; see Fig. 4.

Clearly, the system sizes L attainable for the hierarchical lattice are unrealistic for the EA, and the unknown corrections to scaling disfavor any finite size scaling ansatz in comparison to the accuracy obtained in a simple extrapolation of $p=1$ data.^{35,43} Yet, the striking similarities in the behavior of the data for defect energies of the hierarchical lattice and EA should be noted. The Gaussian bond distribution results in extended transient behavior until scaling is reached, making it impractical to extract the stiffness exponent γ for the EA, even if an optimization heuristic would be applied that could handle remainder graphs beyond the limit of ≈ 250 spins used here. Conversely, the crossover at intermediate p for system size corrections minimizes transient behavior for $\pm J$ bonds, leading to the best data collapse for values of L realistic achievable for the EA. This intermediate window in p is invariant but narrows for $d \rightarrow \infty$, allowing for reasonable determinations of γ_d for as high a dimension as $d=7$, with scaling in the data collapse extending over two decades in $d=3$ to merely half a decade in $d=7$.²⁸ These new values for γ_d allow for a direct comparison with mean field predictions.⁴⁶ Our study here should add some confidence into those findings.

ACKNOWLEDGMENTS

S.B. would like to thank A. Bray and M. Moore for helpful discussions. This work was supported by NSF Grant No. DMR-0312510.

*Electronic address: www.physics.emory.edu/faculty/boettcher

¹ *Spin Glasses and Random Fields*, edited by A. P. Young (World Scientific, Singapore, 1997).

² *Landscape Paradigms in Physics and Biology*, edited by H. Frauenfelder *et al.* (Elsevier, Amsterdam, 1997).

³ P. Sibani and J. Dall, *Eur. Phys. J. B* **36**, 233 (2003).

⁴ S. Boettcher and P. Sibani, cond-mat/0406543 (unpublished).

⁵ *New Optimization Algorithms in Physics*, edited by H. Rieger and A. Hartmann (Springer, Berlin, 2004).

⁶ S. F. Edwards and P. W. Anderson, *J. Phys. F: Met. Phys.* **5**, 965 (1975).

⁷ K. H. Fischer and J. A. Hertz, *Spin Glasses* (Cambridge University Press, Cambridge, England, 1991).

⁸ D. Sherrington and S. Kirkpatrick, *Phys. Rev. Lett.* **35**, 1792 (1975).

⁹ G. Parisi, *J. Phys. A* **13**, L115 (1980).

¹⁰ M. Mezard, G. Parisi, and M. A. Virasoro, *Spin Glass Theory and Beyond* (World Scientific, Singapore, 1987).

¹¹ D. S. Fisher and D. A. Huse, *Phys. Rev. Lett.* **56**, 1601 (1986).

¹² F. Barahona, *J. Phys. A* **15**, 3241 (1982).

¹³ M. Mezard, G. Parisi, and R. Zecchina, *Science* **297**, 812 (2002).

¹⁴ E. Marinari and G. Parisi, *Europhys. Lett.* **19**, 451 (1992).

¹⁵ J. Dall and P. Sibani, *Comput. Phys. Commun.* **141**, 260 (2001).

¹⁶ K. F. Pal, *Physica A* **233**, 60 (1996); *Physica A* **223**, 283 (1996).

¹⁷ A. K. Hartmann, *Phys. Rev. E* **59**, 84 (1999).

¹⁸ M. Palassini and A. P. Young, *Phys. Rev. Lett.* **83**, 5126 (1999).

¹⁹ S. Boettcher and A. G. Percus, *Phys. Rev. Lett.* **86**, 5211 (2001).

²⁰ A. A. Middleton, *Phys. Rev. E* **69**, 055701(R) (2004).

²¹ F. Krzakala and O. C. Martin, *Phys. Rev. Lett.* **85**, 3013 (2000).

²² M. Palassini and A. P. Young, *Phys. Rev. Lett.* **85**, 3017 (2000).

²³ A. J. Bray and M. A. Moore, *J. Phys. C* **17**, L463 (1984).

²⁴ A. C. Carter, A. J. Bray, and M. A. Moore, *Phys. Rev. Lett.* **88**, 077201 (2002).

²⁵ B. Drossel and M. A. Moore, *Eur. Phys. J. B* **21**, 589 (2001).

²⁶ A. K. Hartmann and A. P. Young, *Phys. Rev. B* **64**, 180404(R) (2001).

²⁷ S. Boettcher, *Eur. Phys. J. B* **38**, 83 (2004).

²⁸ S. Boettcher, *Europhys. Lett.* **67**, 453 (2004).

²⁹ $T=0$ phase transitions on dilute lattices have been studied in many contexts before, for instance, for the Ising model by M. J. Stephen and G. S. Grest, *Phys. Rev. Lett.* **38**, 567 (1977), or for quantum spin models, see B. K. Chakrabarti, A. Dutta, and P.

- Sen, *Quantum Ising Phases and Transitions in Transverse Ising Models* (Springer, Berlin, 1996).
- ³⁰S. Boettcher and A. K. Hartmann, cond-mat/0503486 (unpublished).
- ³¹C. Amoruso, E. Marinari, O. C. Martin, and A. Pagnani, Phys. Rev. Lett. **91**, 087201 (2003).
- ³²J.-P. Bouchaud, F. Krzakala, and O. C. Martin, Phys. Rev. B **68**, 224404 (2003).
- ³³A. J. Bray and S. Feng, Phys. Rev. B **36**, 8456 (1987).
- ³⁴T. Jorg, cond-mat/0410328 (unpublished).
- ³⁵S. Boettcher, Eur. Phys. J. B **33**, 439 (2003).
- ³⁶J. R. Banavar, A. J. Bray, and S. Feng, Phys. Rev. Lett. **58**, 1463 (1987).
- ³⁷S. Boettcher and E. Marchetti (unpublished).
- ³⁸A. A. Migdal, Sov. Phys. JETP **42**, 743 (1975); L. P. Kadanoff, Ann. Phys. (N.Y.) **100**, 359 (1976).
- ³⁹S. Kirkpatrick, Phys. Rev. B **15**, 1533 (1977).
- ⁴⁰B. W. Southern and A. P. Young, J. Phys. C **10**, 2179 (1977).
- ⁴¹O. Beckman, E. Figueroa, K. Gramm, L. Lundgren, K. V. Rao, and H. S. Chen, Phys. Scr. **25**, 726 (1982).
- ⁴²H. Maletta and W. Felsch, Phys. Rev. B **20**, 1245 (1979).
- ⁴³T. Aspelmeier, A. J. Bray, and M. A. Moore, Phys. Rev. Lett. **89**, 197202 (2002).
- ⁴⁴P. H. L. Martins and J. A. Plascak, Phys. Rev. E **67**, 046119 (2003).
- ⁴⁵C. D. Lorenz and R. M. Ziff, Phys. Rev. E **57**, 230 (1998).
- ⁴⁶S. Boettcher, cond-mat/0407130 (unpublished).